LOOP-SHAPING $\mathcal{H}_\infty$ CONTROL OF AN AEROPENDULUM MODEL

Ricardo BREGANON[*] and Uiliam Nelson L.T. ALVES
Instituto Federal do Paraná, Av. Dr Tito, 801, Jacarezinho – PR
Universidade Tecnológica Federal do Paraná, Programa de Pós-Graduação em Engenharia Mecânica
Av. Alberto Carazzai, 1640, Cornélio Procópio – PR, BRAZIL
E-mail: ricardo.breganon@ifpr.edu.br

João Paulo L.S. De ALMEIDA and Fernando S.F. RIBEIRO
Instituto Federal do Paraná, Av. Dr Tito, 801, Jacarezinho – PR, BRAZIL

Marcio MENDONÇA, Rodrigo H.C. PALÁCIOS and Marcio A.F. MONTEZUMA
Universidade Tecnológica Federal do Paraná, Av. Alberto Carazzai, 1640
Cornélio Procópio – PR, BRAZIL

This work presents a mathematical model of an aeropendulum system with two sets of motors with propellers and the design and simulation of a loop-shaping $\mathcal{H}_\infty$ control for this system. In this plant, the objective is to control the angular position of the pendulum rod through the torque generated by the thrust of the motorized propellers at the end of the rod's axis. The control design is obtained by first using feedback linearization and then designing the $\mathcal{H}_\infty$ controller using the resulting linear system. For the control strategy validation, simulations were conducted in the Matlab/Simulink® environment, and the weighting functions for the $\mathcal{H}_\infty$ controller were adjusted to obtain the desired performance and stability of the closed-loop system. The simulation results show the efficiency of the applied methodology.

Key words: dynamic system modeling, aeropendulum, $\mathcal{H}_\infty$ control.

1. Introduction

Inverted pendulum systems present high dynamic complexity and represent a challenge in the automatic control field due to their nonlinearity and unstable equilibrium point when the pendulum rod is at the vertical position (Ogata [1]). Several approaches and configurations of inverted pendulums are studied in the literature, such as the Furuta pendulum (Furuta *et al.* [2]; Antonio-Cruz *et al.* [3]; Zabihifar *et al.* [4]), the cart pendulum (Blondin and Pardalos [5]; Roose, Yahya and Al-Rizzo [6]), the robot pendulum (Grasser *et al.* [7]; Ye *et al.* [8]; Johnson *et al.* [9]), the single propeller pendulum (Job and Jose [10]; Habib *et al.* [11]), among others. The aeropendulum system with two propellers has been also analyzed, which presents a dynamic behavior similar to the traditional helicopters and can be used as a didact tool for engineering studies (Saleem *et al.* [12]).

From a constructive perspective, the aeropendulum considered in this paper is a system composed of a pendulum rod with two sets of motors with propellers at its free extremity, while the other rod extremity is coupled to a rotational axis, which has an encoder to measure the angular position of the rod. In the literature, Saleem *et al.* [12] use an adaptive Proportional-Integrative-Derivative (PID) controller for a system similar to this, where a Particle Swarm Optimization (PSO) and Fuzzy inference system algorithms were used to tune

---

[*] To whom correspondence should be addressed

the gains of the controller. Similar equipment is also considered in Jaber *et al.* [13], where a geometric non-linear controller is presented, in Ghanbari *et al.* [14], where a continuous controller of sampled data is used, and in Gultekin and Tascioglu [15], that uses a PD controller.

The $\mathcal{H}_\infty$ control technique can be applied to several mechanical systems due to its robust performance, even when the system's model presents uncertainties or different types of disturbances. For example, Sampaio *et al.* [16] present an $\mathcal{H}_\infty$ controller to stabilize a quadrotor with 2 degrees of freedom (DOF); Breganon *et al.* [17] propose an $\mathcal{H}_\infty$ controller to control the position and orientation of a Stewart platform with 6 DOF.

Based on the wide range of investigation and application of aeropendulum systems, the importance assigned to the control technique studies applied to this type of system can be noticed. In this way, the main objective of this work is to present the mathematical model, an $\mathcal{H}_\infty$ controller design for the position control, and simulation results of an aeropendulum system that uses two sets of motorized propellers.

The paper is divided as follows: in Section 2, the mathematical model of the aeropendulum, its main parameters, and the use of feedback linearization are presented. In Section 3, the $\mathcal{H}_\infty$ controller design is described. The main simulation results and discussions are conducted in Section 4. Finally, the conclusions and perspectives for future works are presented in Section 5.

2. Aeropendulum system's modeling

The methodology for mathematical modeling and the parameters' obtainment of an aeropendulum system are described in this section. The considered aeropendulum model is based on the one available at the Automation Laboratory of the Instituto Federal do Paraná (IFPR) – Jacarezinho.

2.1. Mathematical model

Let us consider an aeropendulum system shown in Fig.1., where $m_1 = 0.02kg$ represents the rod's mass, $m_2 = 0.295kg$, the mass of the motorized propellers, $2l_1$ ($l_1 = 0.1465m$) indicates the rod's length, $l_2 = 0.306m$, the distance between the rotation axis and the center of mass of the motorized propellers, and $m_c = 0.045kg$ is the mass of the rod's coupling cylinder as well as $r_1 = 0.02m$ and $r_2 = 0.004m$ are its larger and smaller radius, respectively. In summary, this system consists of a rod in which one extremity is coupled to a rotational axis, and the other one (free extremity) has two sets of motorized propellers. Thus, the motors generate torque to the system through the thrust generated by the propellers. In this work, it is considered that the independent actuation of each motorized propeller provides a resultant thrust that defines the rotation movement of the pendulum rod.

For the mathematical modeling, it is considered that the thrust provided by the motorized propellers generates a force at the free extremity of the rod. Thus, Newton's second law and the D'Alembert principle are used to describe the system motion equation, which led to

$$\left(\frac{1}{3}m_1\left(2l_1\right)^2 + m_2l_2^2 + \frac{1}{2}m_c\left(r_1^2 + r_2^2\right) \right)\ddot{\theta}(t) = -\left(m_1l_1 + m_2l_2\right)g\sin\left(\theta(t)\right) - b\dot{\theta}(t) + \tau(t), \quad (2.1)$$

in which the first term comes from the system's inertial moment; the second term is the torque due to the weight of the pendulum set; the third term is the torque due to the viscous friction of the bearings and to the aerodynamic drag caused by the propeller; and the last term is the torque provided by the motorized propellers' thrust (Gultekin and Tascioglu [15]). $\theta(t)$ represents the rotational angle of the pendulum, g is the acceleration due to gravity, and $\tau(t)$ is the torque generated by the thrust due to the propeller's actuation.
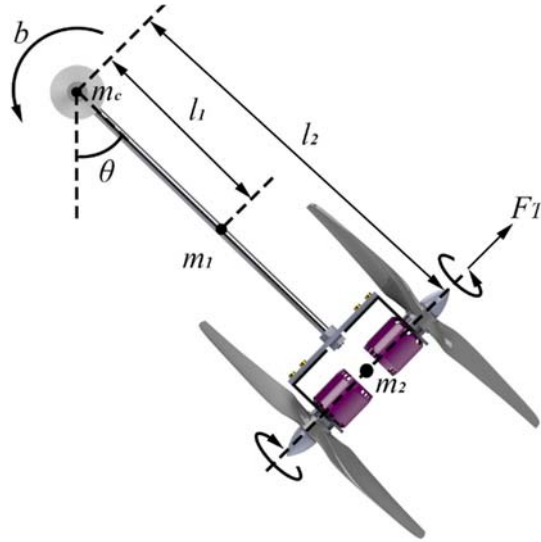
Fig.1. A simplified scheme of an aeropendulum system.

One can observe that (2.1) is nonlinear due to the term $(m_1l_1 + m_2l_2)g\sin(\theta(t))$. In this work, to simplify the design procedure, the linearization of the model (2.1) is carried out by feedback linearization. Thus, the torque applied to the system is defined as

$$\tau(t) = (m_1l_1 + m_2l_2)g\sin(\theta(t)) + u(t) \tag{2.2}$$

where $u(t)$ is the control signal. By substituting (2.2) into (2.1), we have

$$\left(\frac{1}{3}m_1(2l_1)^2 + m_2l_2^2 + \frac{1}{2}m_c\left(r_1^2 + r_2^2\right)\right)\ddot{\theta}(t) = -b\dot{\theta}(t) + u(t) \tag{2.3}$$

and by taking the Laplace transform of (2.3) it results in the transfer function given by

$$G_n(s) = \frac{\Theta(s)}{U(s)} = \frac{\dfrac{1}{J}}{s^2 + \dfrac{b}{J}s} \tag{2.4}$$

where $\Theta(s)$ represents the Laplace transform of the rod's angle $\theta(t)$, $U(s)$ is the Laplace transform of the control signal $u(t)$, and $J = \left(\frac{1}{3}m_1(2l_1)^2 + m_2l_2^2 + \frac{1}{2}m_c\left(r_1^2 + r_2^2\right)\right) = 0.0282\left[kg \cdot m^2\right]$.

2.2. Obtaining the system's parameters

The majority of the parameters required by the mathematical model of the aeropendulum were obtained from an actual prototype, which is shown in Fig.2.

The viscous friction of the pendulum (parameter b in (2.4)) was obtained through an experiment considering the free-swinging movement of the rod. In this experiment, from the resting position (free

extremity pointing downwards), the rod was brought manually to a small angle (about *0.4267* rad) and then released such that the oscillatory dynamics of the system were observed. It is important to highlight that in this initial experiment, the aeropendulum behaved as a simple pendulum system, in which there is an initial condition given by the angle $\theta(0)$ (a small inclination angle), and the only force acting on the system is the force of gravity $g = 9.81m/s^2$. The oscillation obtained from this experiment is shown in Fig.3., and the data (time and value) of the first three peaks are shown in Tab.1.

The total moment of inertia consists of the sum of the individual moments of the rod, the motorized propellers set, and the coupling cylinder between the rod and the rotational axis. Thus, it is described by

$$J = \left(\frac{1}{3}m_1\right)(2l_1)^2 + m_2l_2^2 + \frac{1}{2}m_c\left(r_1^2 + r_2^2\right) \tag{2.5}$$

where r_1 and r_2 are the larger and smaller radius, respectively, of the coupling cylinder between the rod and the rotational axis, whose mass is denoted by m_c.

Fig.2. Aeropendulum prototype available at the Automation Laboratory of Instituto Federal do Paraná, Jacarezinho, Paraná, Brazil.

Table 1. Data obtained from the free-swinging movement of the aeropendulum shown in Fig.3.

Time [s]	Angle [rad]
$t_0 = 0$	$y_0 = 0.4267$
$t_1 = 1.1$	$y_1 = 0.3691$
$t_2 = 2.18$	$y_2 = 0.3063$

By applying Newton's law for rotation on the system shown in Fig.1. it yields

$$J\ddot{\theta}(t) + m_1gl_1\sin(\theta(t)) + m_2gl_2\sin(\theta(t)) + b\dot{\theta}(t) = 0. \tag{2.6}$$

For small values of $\theta(t)$, the approximation $\sin(\theta(t)) \approx \theta(t)$ can be carried out. By the change of variables $a_1 = b/J$ and $a_2 = g(m_1l_1 + m_2l_2)/J$, (2.6) becomes

$$\ddot{\theta}(t) + a_1 \dot{\theta}(t) + a_2 \theta(t) = 0. \tag{2.7}$$

The null input response of a system described by (2.7) is obtained from its characteristic equation $D^2 + a_1 D + a_2 = 0$ (Lathi, [18]). If $a_1^2 - 4 \times a_2 < 0$, then the characteristic equation of the system has the roots $\alpha \pm j\beta$, which is given by

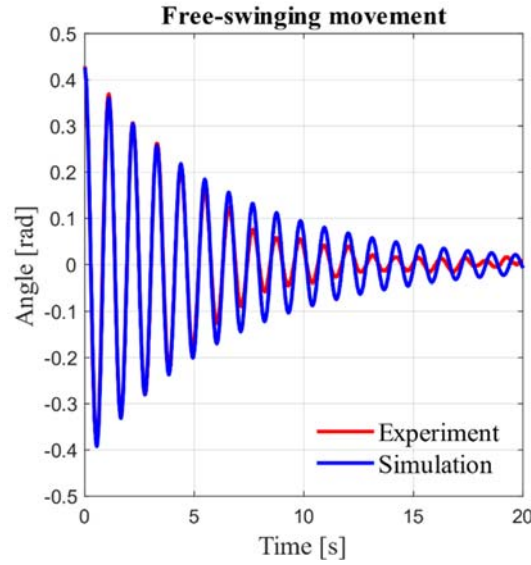$$\alpha \pm j\beta = \frac{-a_1}{2} \pm j \frac{\sqrt{a_1^2 - 4 \times a_2}}{2}. \tag{2.8}$$

Fig.3. Time response of the aeropendulum system during its free-swinging movement.

In this case, the null input response of the system (2.7) has the form (Lathi [18]):

$$y_0(t) = A e^{\alpha t} \cos(\beta t + \phi) \tag{2.9}$$

where A and ϕ are parameters that depend on the initial conditions. Note that the maximum values occur when $\cos(\beta t + \phi) = 1$. From the first three maximum points in the time response shown in Fig.3., described in Tab.1., and from (2.9), one has

$$A e^{\alpha t_1} = y_1, \qquad A e^{\alpha t_2} = y_2. \tag{2.10}$$

By dividing the equations in (2.10), it follows

$$e^{\alpha t_1 - \alpha t_2} = \frac{y_1}{y_2}, \qquad \alpha(t_1 - t_2) = \ln\left(\frac{y_1}{y_2}\right), \qquad \alpha = \frac{\ln\left(\dfrac{y_1}{y_2}\right)}{(t_1 - t_2)}. \tag{2.11}$$

The frequency β is obtained from the period in the response shown in Fig.3. by

$$\beta = \frac{2\pi}{t_2 - t_1}. \qquad (2.12)$$

Furthermore, from (2.8) and (2.11), and the data in Tab.1., one finds

$$a_1 = -2\alpha = 0.3045 \qquad (2.13)$$

and

$$(\beta \times 2)^2 = a_1^2 + 4 \times a_2, \qquad a_2 = \frac{(2\beta)^2 + a_1^2}{4} = 33.257. \qquad (2.14)$$
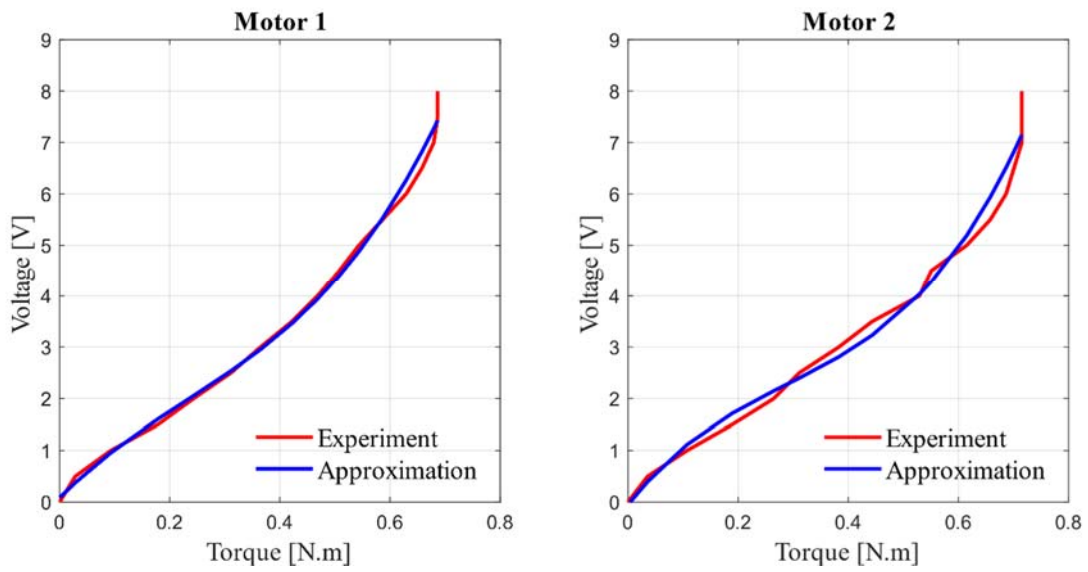

Fig.4. Relationship between voltage and torque of the motorized propellers.

Thus, $b = a_1 \times J = 0.0086\ Nms / rad$. By substituting these values in (2.4), it follows that

$$G_n(s) = \frac{\Theta(s)}{U(s)} = \frac{35.46}{s^2 + 0.305s}. \qquad (2.15)$$

The mathematical model presented in (2.1) considers the torque as the control input. However, this torque is provided by the sets of motorized propellers that are activated by voltage levels. Thus, the real constraints of the control signal encompass the voltage limits of the motors. The relationship between these variables was identified considering the actual prototype to convert the torque signal into its corresponding voltage level. The data from the real prototype is shown in Fig.4. as well as its approximation.

The relationship between torque and voltage levels presented in Fig.4. was used to estimate the voltage applied to the simulated motors, considering the saturation levels. Although both motorized propellers have the same dimensions and electrical characteristics, it is possible to see that each set of motorized propellers has a slightly different response. A third-degree polynomial was used to model the presented response curves

by employing *polyfit* tool available in the Matlab® software. The polynomials obtained for the left $(V(\tau_1))$ and right $(V(\tau_2))$ motor are described as

$$\begin{bmatrix} V(\tau_1) \\ V(\tau_2) \end{bmatrix} = \begin{bmatrix} 24.1725\tau_1^3 - 16.6195\tau_1^2 + 10.7176\tau_1 + 0.0839 \\ 33.1576\tau_2^3 - 28.5849\tau_2^2 + 13.5630\tau_2 - 0.05 \end{bmatrix}. \tag{2.16}$$

3. $\mathcal{H}_\infty$ control

The standard $\mathcal{H}_\infty$ problem is formulated in order to find a $K(s)$ controller, if one exists, such that the closed-loop system is stable and presents the desired performance. A typical diagram of a feedback SISO system is presented in Fig.5. (Oliveira, Aguiar and Vargas [19]; Doyle *et al.* [20]; Zhou, Doyle and Glover [21]).
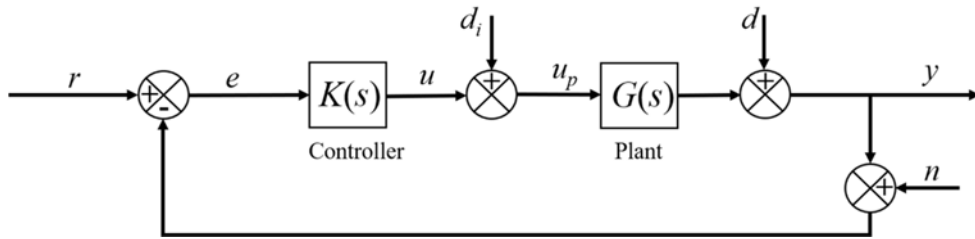

Fig.5. Typical diagram of a feedback system (adapted from Oliveira, Aguiar and Vargas [19]).

From the block diagram presented in Fig.5., the following equations are obtained:

$$e = r - y = S(r - d) + Tn + SGd_i, \tag{3.1}$$

$$u = KS(r - n - d) + Sd_i \tag{3.2}$$

where d_i is the plant's input disturbance, d is the output's disturbance, and n represents sensor's noises. The sensitivity matrix $S(s)$ and the complementary sensitivity matrix $T(s)$ are given by

$$S(s) = (I + G(s)K(s))^{-1}, \tag{3.3}$$

$$T(s) = G(s)K(s)(I + G(s)K(s))^{-1} = I - S(s). \tag{3.4}$$

In the servo system design, it is desired that the error (e) be null and, consequently, the plant's output follows the reference signal. From (3.1), for e to be small compared to the disturbances d, d_i, and also to the reference r, $S(s)$ must be small. On the other hand, in order to obtain a small effect of the noise n on the error e, $T(s)$ must be small. However, $T(s) + S(s) = I$ and then it is not possible to reach both of the mentioned objectives at the same frequency range, simultaneously. Another critical point in the controller design is the magnitude of the control signal u, which must be small in order to stay within the physical constraints of the system (within the saturation limits). From (3.1), this can be achieved if, in addition to S,

KS has a small amplitude. The size of the complex functions is understood through its $\mathcal{H}_\infty$ norm, which is defined as

$$\|S\|_\infty = \sup_\omega |S(j\omega)|. \tag{3.5}$$

Thus, in the specifications for attenuation of disturbance and steady-state error, generally, an upper limit for the norm of $S(j\omega)$ is considered, that is:

$$|S(j\omega)| \le |W_1^{-1}(j\omega)|, \qquad \forall\omega, \tag{3.6}$$

in which $W_1(j\omega)$ ponders $S(j\omega)$ and reflects the desired attenuation for each frequency ω.

From (3.2), a constraint on the control signal $u(t)$ can be introduced by a bound on $K(j\omega)S(j\omega)$, which can be given by

$$|K(j\omega)S(j\omega)| \le |W_2^{-1}(j\omega)|, \qquad \forall\omega, \tag{3.7}$$

such that the function $W_2(j\omega)$ limits the control input within an acceptable range, avoiding the saturation.

Suppose that the plant $G(s)$ has multiplicative uncertainties so that it can be described by

$$G(s) = [1 + W(s)\Delta(s)]G_n(s) \tag{3.8}$$

where $\|\Delta\|_\infty \le 1$ and $G_n(s)$ is the nominal model of the system. Thus, $K(s)G(s) = K(s)[1 + W(s)\Delta(s)]G_n(s) = K(s)G_n(s) + K(s)W(s)\Delta(s)G_n(s)$.

By analysing the Nyquist diagram for the nominal system, the distance between $K(s)G_n(s)$ and the critic point $-1 + j0$ is given by $|K(j\omega)G_n(j\omega) + 1|$ (Oliveira, Aguiar and Vargas [19]). Therefore, to avoid an involvement of the critical point, the distance between $K(j\omega)G_n(j\omega)$ and -1 must be greater than the uncertainty module $|K(j\omega)W(j\omega)\Delta(j\omega)G_n(j\omega)|$. Thus,

$$|K(j\omega)W(j\omega)\Delta(j\omega)G_n(j\omega)| \le |K(j\omega)W(j\omega)G_n(j\omega)| < |K(j\omega)G_n(j\omega) + 1|,$$
$$\left|\frac{K(j\omega)W(j\omega)G_n(j\omega)}{K(j\omega)G_n(j\omega) + 1}\right| < 1 \tag{3.9}$$

and, from (3.4),

$$|W(j\omega)T(j\omega)| < 1 \tag{3.10}$$

which must be valid for any ω. In this way, the size of the smaller disturbance $W(j\omega)$ described by a multiplicative uncertainty (3.5) that makes the feedback system unstable is given by

$$\|W(s)\|_{\infty} = \frac{1}{\|T(s)\|_{\infty}}. \tag{3.11}$$

That is, a small value of $\|T(s)\|_{\infty}$ corresponds to a high value for the destabilizing uncertainty and leads to a greater stability margin. As a consequence, an upper limit for $\|T(s)\|_{\infty}$ can be specified as

$$|T(j\omega)| \le |W_3^{-1}(j\omega)|, \quad \forall \omega \tag{3.12}$$

where the function $W_3(j\omega)$ minimizes the peak of the complementary sensitivity function $T(s)$ so that oscillations are mitigated, and stability is guaranteed. However, $W_3(j\omega)$ and $W_1(j\omega)$ specifications conflict, especially at low frequencies, due to the relation $S(j\omega) + T(j\omega) = I$.

The constraints described by (3.6), (3.7), and (3.12) can be understood as a restriction in the $\mathcal{H}_{\infty}$ norm of an augmented plant based on the diagram of Fig.5. The augmented plant with the weighting functions is presented in Fig.6., in which $w(t)$ and $u(t)$ are the augmented system's inputs, while $z_1(t)$, $z_2(t)$, and $z_3(t)$ are the outputs. In this diagram, $w(t)$ and $u(t)$ correspond to the reference r and the control signal $u(t)$ as defined in Fig.5., respectively.
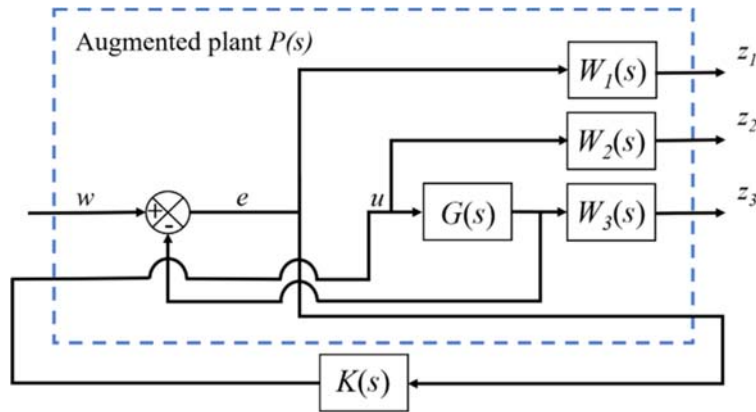

Fig.6. Augmented plant for the $\mathcal{H}_{\infty}$ controller (adapted from Oliveira, Aguiar and Vargas [19]).

The relation between the inputs and outputs of the augmented plant of Fig.6. is given by

$$\begin{bmatrix} z_1 \\ z_2 \\ z_3 \\ e \end{bmatrix} = \begin{bmatrix} W_1 & -W_1 G \\ 0 & W_2 \\ 0 & W_3 G \\ I & -G \end{bmatrix} \begin{bmatrix} w \\ u \end{bmatrix} = P(s) \begin{bmatrix} w \\ u \end{bmatrix}. \tag{3.13}$$

From the diagram of Fig.6. and considering the output vector $z = \begin{bmatrix} z_1 & z_2 & z_3 \end{bmatrix}^T$ and the input w, the transfer function matrix T_{zw} is given by

$$T_{zw} = \begin{bmatrix} W_1 S \\ W_2 KS \\ W_3 T \end{bmatrix} \tag{3.14}$$

and the norm constraints defined in (3.6), (3.7), and (3.12) can be described by means of a bound in the $\mathcal{H}_\infty$ norm of T_{zw} such that

$$\left\| T_{zw} \right\|_\infty = \left\| \begin{matrix} W_1 S \\ W_2 KS \\ W_3 T \end{matrix} \right\|_\infty \leq \gamma. \tag{3.15}$$

The following weighting functions were considered in the designing of the controller

$$W_1 = \frac{0.1125}{s + 0.0025}, \qquad W_2 = \frac{0.27s + 5.4}{s + 50} \tag{3.16}$$

with the objective of minimizing the steady-state error and the constraints about the control input, respectively. The weighting function W_3 was not used in this work because no uncertainty parameter was considered in the simulated system.

The augmented plant $P(s)$, from (3.13), considered in this work was obtained with the function *augtf* of Matlab®. This plant is described in state space by the following matrices:

$$A = \begin{bmatrix} -0.305 & 0 & 0 & 0 \\ 0.5 & 0 & 0 & 0 \\ 0 & -8.867 & -0.0025 & 0 \\ 0 & 0 & 0 & -50 \end{bmatrix}, \qquad B = \begin{bmatrix} 0 & 8 \\ 0 & 0 \\ 1 & 0 \\ 0 & 1 \end{bmatrix},$$

$$C = \begin{bmatrix} 0 & 0 & 0.1125 & 0 \\ 0 & 0 & 0 & -8.1 \\ 0 & -8.867 & 0 & 0 \end{bmatrix}, \qquad D = \begin{bmatrix} 0 & 0 \\ 0 & 0.27 \\ 1 & 0 \end{bmatrix}. \tag{3.17}$$

The $\mathcal{H}_\infty$ controller's gain ($K(s)$) designed for the aeropendulum were obtained using the function *hinf* of Matlab®, and it is described in state space by the following matrices:

$$A_c = \begin{bmatrix} -8.85 & -3.798 & 32.06 & -23.47 \\ -1.24 & -0.6144 & 5.28 & -3.909 \\ 0.923 & 0.9955 & -10.64 & 10.21 \\ -1.383 & 0.2054 & 1.114 & -6.558 \end{bmatrix}, \qquad B_c = \begin{bmatrix} 0.05739 \\ -1.342 \\ -0.6846 \\ -0.6302 \end{bmatrix},$$

$$C_c = \begin{bmatrix} 1.372 & 0.6096 & -5.165 & 3.776 \end{bmatrix}, \qquad D_c = \begin{bmatrix} 0 \end{bmatrix}. \tag{3.18}$$

The Bode diagram of $W_1(j\omega)^{-1}$ and the sensitivity funtion $S(j\omega)$ are presented in Fig.7(a), while the Bode diagram of $W_2(j\omega)^{-1}$ and $K(j\omega)S(j\omega)$ are shown in Fig.7(b). It is possible to notice that the constraints (3.6) and (3.7) were satisfied for the obtained $\mathcal{H}_\infty$ controller.
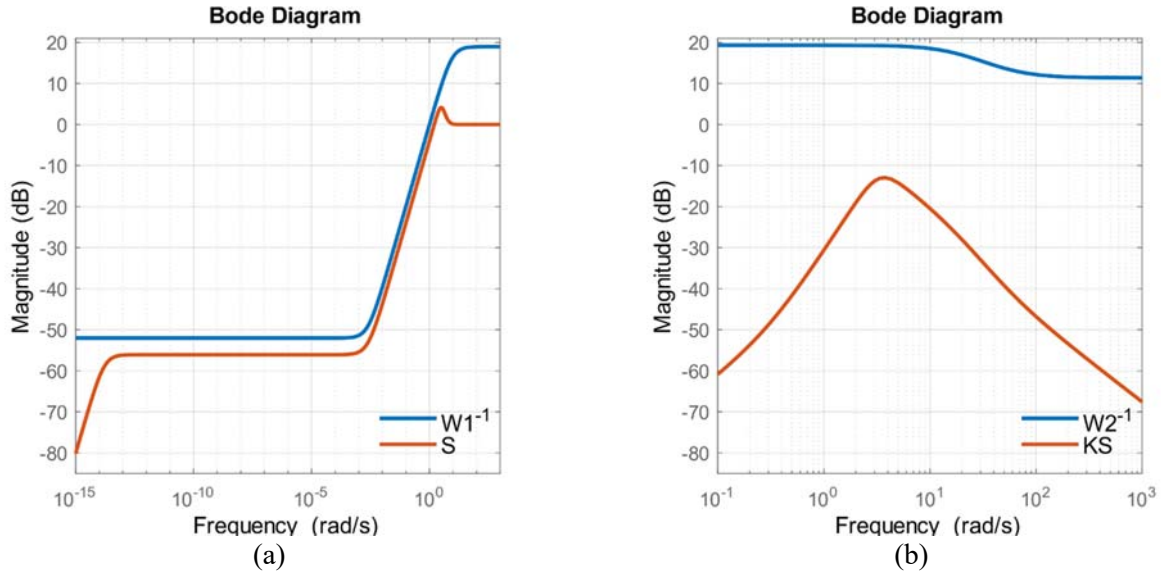

Fig.7. Bode diagrams of the weighting functions $W_1(j\omega)^{-1}$ and $W_2(j\omega)^{-1}$, inverse of (3.16), $S(j\omega)$ and $K(j\omega)S(j\omega)$.

4. Simulation results

The control diagram of Fig.8. was considered for the simulation of the aeropendulum system with the $\mathcal{H}_\infty$ controller, where $K(s)$ is given in state space by (3.18).
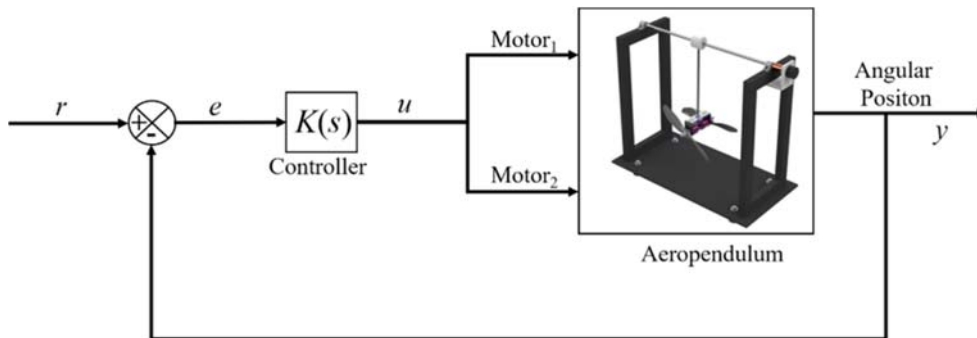

Fig.8. Control system diagram for the aeropendulum simulation.

Initially, a step reference with an amplitude of π rad ($r = \pi$ rad) at 1 second was considered in the simulation. In this first experiment, the system's response (Fig.9(a)) presents a peak value of about *3.386* rad, representing an overshoot of *7.78%* concerning the reference, and the stabilization time is about *5.998* seconds. In Fig.9(b), it is possible to see the error tending to zero.
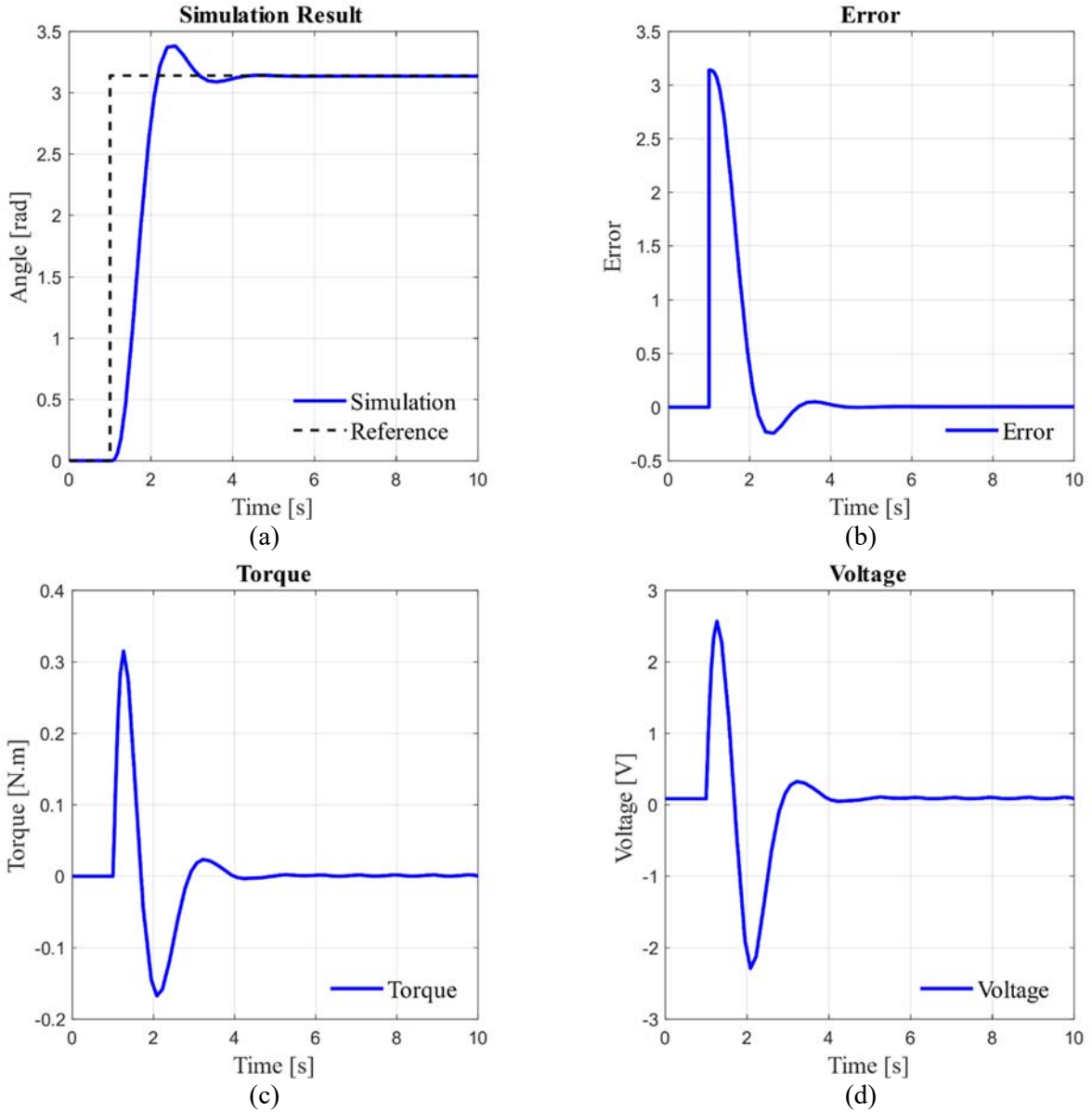
Fig.9. System's response to the step reference ($r = \pi$ rad) in $t = 1$ s.

The time response of the torque and voltage are presented in Fig.9(c) and (d), respectively. Notice that the torque is the control input in (2.4), whereas the voltage was obtained by the polynomial approximation described in (2.15). In addition, the control action had a low maximum value due to the use of $W_2(s)$ given in (3.16) in the design procedure.

In the second simulation, a sequence of step references with different amplitudes was considered to the system: $r = \left(\dfrac{\pi}{6}, \dfrac{\pi}{3}, \dfrac{\pi}{2}, \dfrac{2\pi}{3}, \dfrac{5\pi}{6}, \pi \right)$ rad applied at instants $t = (10, 20, 30, 40, 50, 60)$ s, correspondingly. The time response of the rod's angle, error, torque provided by the motorized propellers and its equivalent voltage are presented in Figs 10(a) – (d), respectively.

It is possible to observe in Fig.10(a) that the designed controller performed satisfactorily to the reference steps. In other words, it was able to achieve rod stabilization at all desired levels. Complementary,

this fact can also be observed through the error evolution (error tending to zero) in Fig.10(b). Moreover, there were no abrupt variations in the control action, as shown in Figs 10(c) and (d), contributing to the devices' longevity.
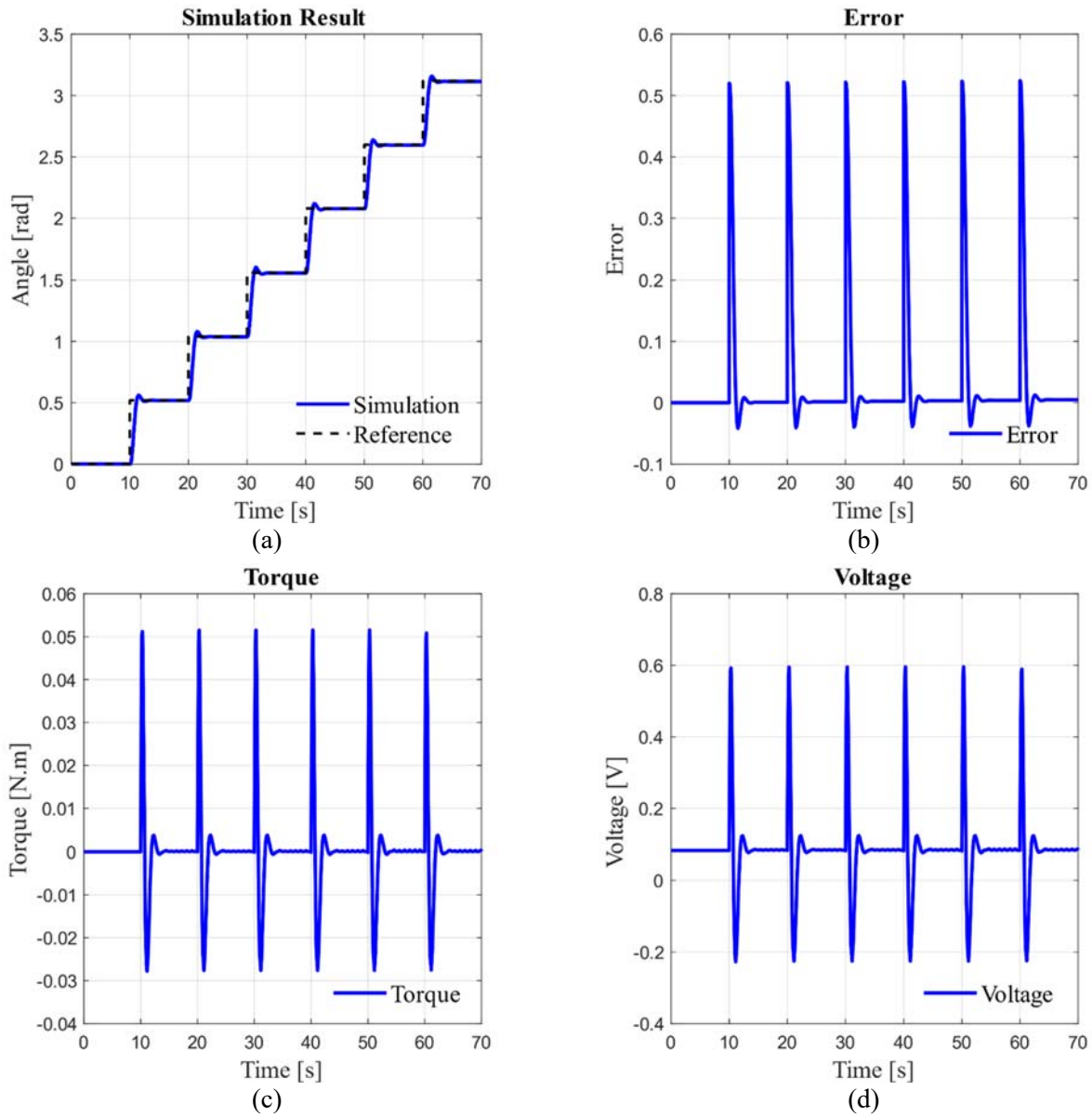

Fig.10. System' response to the reference $r = \left(\dfrac{\pi}{6}, \dfrac{\pi}{3}, \dfrac{\pi}{2}, \dfrac{2\pi}{3}, \dfrac{5\pi}{6}, \pi \right)$ rad in $t = (10, 20, 30, 40, 50, 60)$ s .

5. Conclusions

This work presented an $\mathcal{H}_\infty$ controller design for an aeropendulum system with two motorized propellers using its mathematical model. The main objective was to control the angular position of the aeropendulum through the thrust variation provided by the propellers. The methodology considered for the

mathematical modeling and the project of the $\mathcal{H}_\infty$ controller was validated through simulations in two different scenarios.

In the first set of simulations, a step reference with π rad of amplitude was considered for the pendulum's rod. From the presented results, it was observed that the controller was able to stabilize the pendulum at the desired angle with an adequate stabilization time, despite an overshoot of about *7.78%*.

In the other set of simulations, a sequence of step references with different amplitudes was considered to observe the system's response under successive reference variations. In this case, the efficient performance of the designed controller was also observed, controlling the pendulum at the desired stabilization points and without abrupt variations in the control action.

In future works, the authors intend to apply the $\mathcal{H}_\infty$ controller in the actual prototype to validate both the mathematical model and the control strategy in experiments. This next step is important because these new experiments will naturally encompass unpredictable situations present in any real system, such as noises, disturbances, asymmetries in constructive parts of the actual system, among others.

Acknowledgment

Nomenclature

A – amplitude of the null input response of the aeropendulum system

A,B,C,D – state space matrices of the augmented plant

A_C,B_C,C_C,D_C – state space matrices of the $\mathcal{H}_\infty$ controller

a_1 – characteristic equation coefficient

a_2 – characteristic equation coefficient

b – viscous friction

D – differential operator

d – output's disturbance

d_i – plant's input disturbance

e – error

G – plant

G_n – nominal model of the system

g – gravitational acceleration

I – identity matrix

J – total moment of inertia

K – $\mathcal{H}_\infty$ controller

l_1 – distance from the center of mass of the rod to the rotational axis

l_2 – distance between the rotational axis and the center of mass of the sets of motorized propellers

m_1 – rod's mass

m_2 – mass of the set of motorized propellers

m_c – mass of the rod's coupling cylinder

n – sensor's noises

P – augmented plant

r – reference

r_1 – larger radius of the rod's coupling cylinder

r_2 – smaller radius of the rod's coupling cylinder

S – sensitivity matrix

T – complementary sensitivity matrix

T_{zw} – transfer function between w and z

U – Laplace transform of the control signal

u – control signal

$V(\tau_1)$ – polynomial approximation for the left motor

$V(\tau_2)$ – polynomial approximation for the right motor

y – system output

y_0 – first peak

y_1 – second peak

y_2 – third peak

W_1, W_2, W_3 – weighting functions

z_1, z_2, z_3 – augmented system's outputs

α – attenuation coefficient

β – frequency of the null input response of the aeropendulum system

θ – rotational angle of the pendulum

Θ – Laplace transform of the rod's angle

τ – torque

ϕ – phase of the null input response of the aeropendulum system

References

[1] Ogata Katsuhiko (2010): *Modern Control Engineering.*– Prentice Hall do Brasil.

[2] Furuta K., Yamakita M. and Kobayashi S. (1992): *Swing-up control of inverted pendulum using pseudo-state feedback.*– Journal of Systems and Control Engineering, vol.206, No.6, pp.263-269.

[3] Antonio-Cruz M., Hernadez-Guzman V.M. and Silva-Ortigoza R. (2018): *Limit cycle elimination in inverted pendulums: furuta pendulum and pendubot.*– IEEE Access, vol.6, pp.30317-30332,

[4] Zabihifar S.H., Yushchenko A.S. and Navvabi H. (2020): *Robust control based on adaptive neural network for Rotary inverted pendulum with oscillation compensation.*– Neural Computing and Applications, vol.32, pp.14667-14679.

[5] Blondin M.J., Pardalos P.M. (2020): *A holistic optimization approach for inverted cart-pendulum control tuning.*– Soft Computing, vol.24, pp.4343-4359.

[6] Roose A.I., Yahya S. and Al-Rizzo H. (2017): *Fuzzy-logic control of an inverted pendulum on a cart.*– Computers and Electrical Engineering, vol.61, pp.31-47.

[7] Grasser F., D'Arrigo A., Colombini S. and Rufer A.C. (2002): *JOE: A Mobile, Inverted Pendulum.*– IEEE Transactions on Industrial Electronics, vol.49, No.1, pp.107-114.

[8] Ye W., Li Z., Yang C., Sun J., Su C.Y. and Lu R. (2016): *Vision-based human tracking control of a wheeled inverted pendulum robot.*– IEEE Transactions on Cybernetics, vol.46, No.11, pp.2423-2434.

[9] Johnson T., Zhou S., Cheah W., Mansell W., Young R. and Watson S. (2020): *Implementation of a perceptual controller for an inverted pendulum robot.*– Journal of Intelligent and Robotic Systems, vol.99, pp.683-692.

[10] Job M.M. and Jose P.S.H. (2015): *Modeling and control of mechatronic aeropendulum.*– IEEE Sponsored 2nd International Conference on Innovations in Information Embedded and Communication Systems, vol.978, No.1, pp.1-5.

[11] Habib G., Miklos A., Enikov E.T., Stepan G. and Rega G. (2015): *Nonlinear model-based parameter estimation and stability analysis of an aero-pendulum subject to digital delayed control.*– International Journal Dynamic Control, vol.5, pp.629-643.

[12] Saleem O., Rizwan M., Zeb A.A., Ali A.H. and Saleem M.A. (2019): *Online adaptive PID tracking control of an aero-pendulum using PSO-scaled fuzzy gain adjustment mechanism.*– Soft Computing, Springer, vol.24, pp.10629-10643.

[13] Jaber M., Khan A. and Khan W.A. (2017): *Robust nonlinear geometric angle tracker for aero pendulum.*– Imperial Journal of Interdisciplinary Research, pp.93-99.

[14] Ghanbari M., Bahraini M. and Yazdanpanah M.J. (2018): *Continuous control of sampled data systems with robustness against bounded measurement errors.*– Transactions of the Institute of Measurement and Control, vol.40, No.10, pp.3125-3133.

[15] Gültekin Y. and Tascioglu Y. (2011): *Pendulum positioning system actuated by dual motorized propellers.*– 6 th International Advanced Technologies Symposium, pp.6-11.

[16] Sampaio R.C., Becker M., Siqueira A. A. G, Breganon R., de Salvi F. and Belo E.M. (2011): *Model-based optimal h∞ controller on the stability of a 2-dof Quadrotor.*– Proceedings of the ASME International Design Engineering Technical Conferences and Computers and Information in Engineering Conference. ASME/IEEE International Conference on Mechatronic and Embedded Systems and Applications, Parts A and B. Washington, DC, USA. vol.3., pp.955-962.

[17] Breganon R., Montezuma M.A.F, Souza M.M., Lemes R.C. and Belo E.M. (2018): *Optimal H infinity controller applied to a Stewart platform.*– International Journal of Advanced Engineering Research and Science, vol.5, No.7, pp.51-59.

[18] Lathi B.P. (2007): *Signals and Linear Systems.*– 2 ed. Porto Alegre: Bookman.

[19] Oliveira V.A., Aguiar M.L. and Vargas J.B. (2016): *Control Engineering: Fundamentals and Laboratory Classes.*– Elsevier, Rio de Janeiro.

[20] Doyle J.C., Glover K., Khargonekar P.P. and Francis B.A. (1989): *State-space solutions to standard H2 and H∞ control problems.*– IEEE Transactions on Automatic Control, vol.34, No.8, pp.831-847.

[21] Zhou K., Doyle J.C. and Glover K. (1995): *Robust and Optimal Control.*– Upper Saddle River: Prentice Hall.